geosciences

MDPI

Article

Stratigraphy, Petrography and Grain-Size Distribution of Sedimentary Lithologies at Cahuachi (South Peru): ENSO-Related Deposits or a Common Regional Succession?

Marco Delle Rose [1,*], Michele Mattioli [2], Nicola Capuano [2] and Alberto Renzulli [2]

[1] Istituto di Scienze dell'Atmosfera e del Clima, Consiglio Nazionale delle Ricerche, Complesso Ecotekne, Via per Monteroni, 73100 Lecce, Italy

[2] Dipartimento di Scienze Pure e Applicate, Università degli Studi di Urbino Carlo Bo, Campus Scientifico Enrico Mattei, 61029 Urbino, Italy; michele.mattioli@uniurb.it (M.M.); nicola.capuano@uniurb.it (N.C.); alberto.renzulli@uniurb.it (A.R.)

* Correspondence: m.dellerose@isac.cnr.it; Tel.: +39-0832-298816

Received: 13 December 2018; Accepted: 6 February 2019; Published: 8 February 2019

Abstract: Several central Andean pre-Columbian sites struck by hydrogeological disasters due to El Niño-Southern Oscillation (ENSO) events are reported in the literature. The mainstream explanation for the decline and demise of Cahuachi (*pampa* of Nazca, south Peru) implies the damage and burial of such a ceremonial center as a consequence of two catastrophic river floods, which occurred around 600 CE and 1000 CE, respectively. Therefore, geological studies at Cahuachi are mandatory with regard to both the correlations of ENSO-related deposits ("event-strata") among different Peruvian sites and the assessment of the millennium-scale climate variability. In particular, the latter is crucial to evaluate the environmental and economic consequences due to the incoming fluctuations of ENSO. In this paper, stratigraphic, grain-size distribution, and petrographic investigations on a sedimentary section exposed close to one of the main temples of Cahuachi are reported. They represent the first test for the current mainstream explanation. The preliminary finding indicates that the studied stratigraphic interval may belong to the common regional succession of the *pampa* of Nazca rather than the ENSO-related deposits described in the literature. However, further geological research will be necessary to unravel this issue in more detail.

Keywords: Mega El Niño; *pampa* of Nazca; Cuenca Pisco; Rio Grande de Nazca; grain-size; volcaniclastic layer; stratigraphy; petrography

1. Introduction

Several central Andean pre-Columbian sites struck by hydrogeological disasters due to ENSO (El Niño-Southern Oscillation) events are reported in both the literature in the Earth sciences [1–3] and archaeology [4–6]. Grodzicki [7,8] claims that the ceremonial center of Cahuachi (Rio Grande de Nazca, South Peru) was first severely damaged, then completely buried by catastrophic river floods as a result of two Mega El Niño events, which occurred around 600 Common Era (CE) and 1000 CE, respectively. According to such a hypothesis, each event would be proved by a conglomerate layer. This is based on an interpretative geological setting of the deposits outcropping around the archaeological site, without, however, either geological characterization or direct dating of the main sedimentary lithologies. The ages assigned by Grodzicki to conglomerates were deduced from uncertain stratigraphic relationships with deposits containing materials dated with the ^{14}C method. Despite this uncertainty, the stratigraphic succession of Cahuachi could be a climate proxy-record of

particular interest, especially regarding the millennium-scale climate variability, and thus must be investigated in further detail. Again, several authors have emphasized the correlations of ENSO-related deposits ("event-strata") among different archaeological Peruvian sites [9–11]. These correlations would support the concept of Mega or Super El Niño events [12–14] leading to heavier precipitation phases driven by ENSO, which would hit the central Andean coast with centennial-scale periodicity. It is worth observing that the understanding of the variability of El Niño over geological time is crucial for assessing the environmental and economic consequences due to the incoming fluctuations of ENSO [15–17].

However, before the publication (in 1994) of the *Mapa geologico del cuadrangulo de Palpa* (geological quadrangle map of the Palpa) [18], the geological knowledge of the Rio Grande de Nazca Basin was scarce, and therefore, the thesis of Grodzicki and his group (launched in 1990 and 1992 and then becoming nearly a "paradigm") was difficult to prove. In addition, the lack of large outcrops within the Cahuachi archaeological site hampered the stratigraphic survey of the bedrock. During the 2012 archaeological excavation works at Cahuachi, the geological substratum close to one of the main temple of the site, namely the Piramide Sur, was temporarily exposed. In this way, a stratigraphic study and sampling were carried out, and the grain size features and petrographic analysis were subsequently performed. As a whole, the data collected on the geological bedrock of Piramide (or Temple) Sur first allowed for a comprehensive comparison with nearby Pliocene–Pleistocene deposits, and shed light into the robustness or not of Grodzicki's thesis about the ENSO-related catastrophic river floods, considered for at least three decades as the mainstream and paradigmatic explanation of the demise of Cahuachi as for other pre-Columbian sites for which, however, the hypothesis is better supported by the data [19–22].

2. Geological and Environmental Features

2.1. Regional Setting

Cahuachi is located within the morpho-structural unit named Cuenca Pisco consisting, in turn, of Cordillera de la Costa, Llanuras Costeras, Depresión de Ica-Nasca and Fruente Andino [23]. The Llanuras costeras and the Depresión de Ica-Nasca show flat landscapes, i.e., the *pampas*, due to the sub-horizontal setting of the pre-Quaternary substratum (Figure 1).

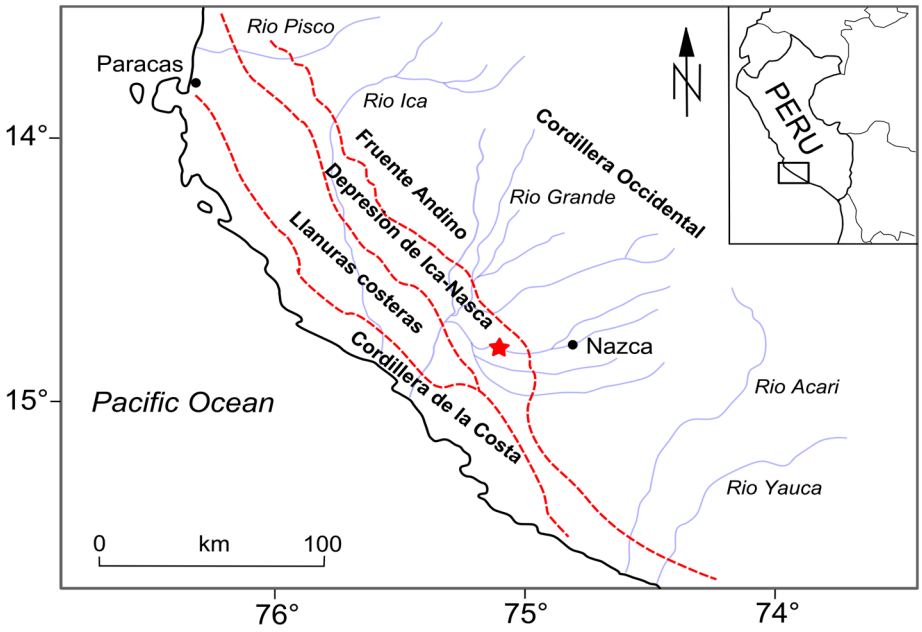

Figure 1. Morpho–structural scheme of the Cuenca Pisco (from [23], modified). The red star indicates the location of Cahuachi.

The Cuenca Pisco gradually emerged from the ocean during the late Pliocene–early Pleistocene, thus evolving from a marginal sea (seaward barred by the ridge of the Cordillera de la Costa) to the present coastal plain. The uplift of the Andes led to abundant supplies of conglomerates that built alluvial fans within the Fruente Andino while planation surfaces and stream terraces formed at the Llanuras Costeras and the Depresión de Ica-Nasca. The lower planation surface has an altitude of about 385 m a.s.l. and a late Middle Pleistocene age (i.e., 200 ka) as determined by cosmogenic ray dating [24]. The regional succession of the *pampa* of Nazca is constituted by the Pisco and Changuillo formations, both of Tertiary age. The plain has an average altitude of about 500 m a.s.l., gently slopes toward the north-west and is bounded by mountain chains of sedimentary and igneous Mesozoic units (Figure 2).

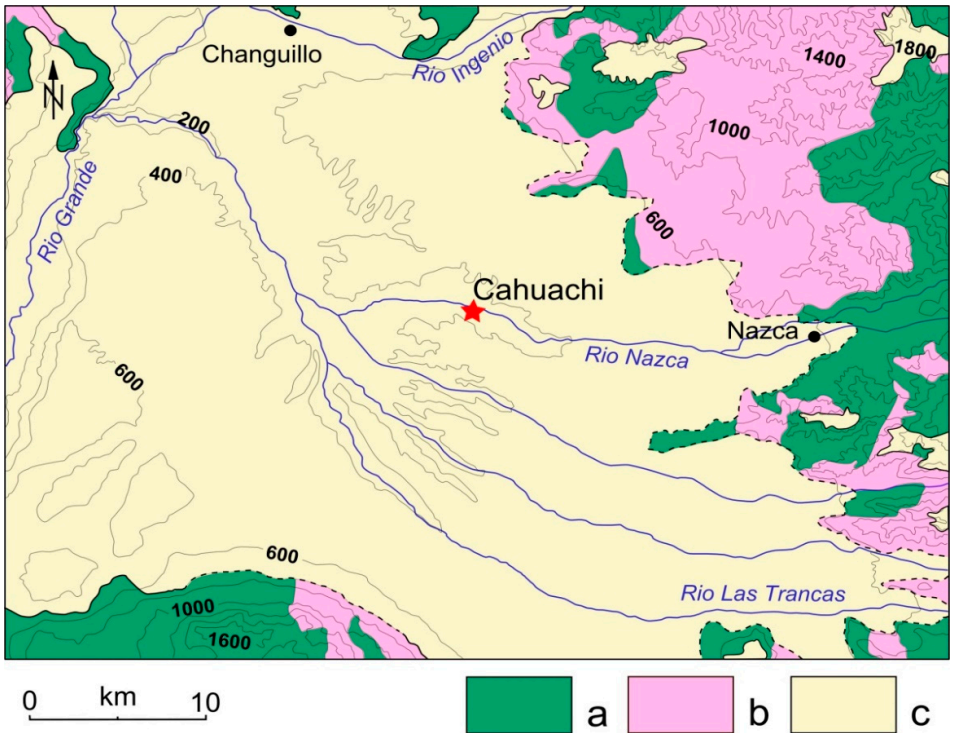

Figure 2. Geological sketch of the *pampa* of Nazca. Legend: (a) marine Jurassic-Cretaceous formations, (b) igneous rocks, (c) marine to continental Tertiary formations (from [18], modified).

The Pisco Formation (Fm) was defined at the beginning of the XIX century during the pioneering geological surveys of the Cuenca Pisco. In contrast, the Changuillo Fm was identified only during the 1980s with the field mapping of the *Mapa geologico del cuadrangulo de Palpa* (geological quadrangle map of the Palpa) [18]. The latter shows a marine to continental transition from the bottom to the top and is constituted by variously-interstratified mudstones, sandstones, breccias and conglomerates. Around Changuillo Village, i.e., the "area-type", some volcaniclastic layers have been found [23]. In several places at the east side of the Cuenca Pisco, conglomerates are prevalent at the top of the Changuillo Fm. Thus, a specific lithostratigraphic unit, named the Canete Fm, has also been defined [23], and is built up by progradational alluvial fans. Along the Cordillera de la Costa, a staircase of terraces represents the corresponding deposits and suggests the episodic uplift of the Dominio Costero. The boundary between the Changuillo and Canete Fms is generally described as transitional while the facies evolve from shallow marine water to shoreface to an alluvial system. Biostratigraphically significant fossils are scarce. The presence of *Carcharodon carcharias*, *Dinocardium nov. sp. Aff.*, and *D. ecuadorialis* suggests a middle–upper Pliocene for the Changuillo Fm [25]. No fossils have been found in the Canete Fm, although an upper Pliocene–lower Pleistocene age can be roughly supposed due to the regional stratigraphic setting [26].

The *pampa* of Nazca belongs to the hyper-arid "chala" life-zone (i.e., the region comprised between the coast and the Andean Precordillera [27]) and constitutes the north-west outlying area of the Atacama Desert. Its environmental conditions are controlled by the SE Pacific anticyclone and the cold Humboldt Current, both inhibiting rainfall. Currently, the annual precipitation is lower than 20 mm, although El Niño-Southern Oscillation may determine significant inter-annual variations. The aridity degree as well as the average impact of El Niño events change along a south–north gradient [28]. Ephemeral or seasonal rivers cross the *pampa* and allow both biological life and human settlements such as the ceremonial center of Cahuachi, which is located on the course of the Nazca River (Figure 2).

Environmental conditions have repeatedly changed over south Peru during the late Quaternary. Starting from the Upper Pleistocene, fluctuations in the moisture transport led to repeated shifts from grassland to desert, and vice versa, on the lower western slopes of the Andes [29]. At the beginning of the Holocene, an increase in easterly precipitation led progressively to persisting vegetation belts in the mountain areas that, in turn, have determined the formation of soils and eolian deposits. About 4.2 ka, the establishment of the modern ENSO atmospheric conditions determined a decrease in precipitation and progressive expansion of deserts. Further environmental changes occurred later as inferred from geomorphological features. Finally, from the end of the last millennium Before the Common Era (BCE) to about 1.3 ka (which is a time interval comprising the rise and decline of the Nasca Culture), alluvial deposits have widely accumulated within the Depresión de Ica-Nasca. Such a process suggests an important hydrological activity [30].

2.2. The Nasca Culture: From the Thriving Period to the Demise

The Nasca Culture arose during the Early Intermediate Period, i.e., around 200 BCE, later spreading its cultural and religious dominance over a large area of southern Peru under the influence of the theocratic capital of Cahuachi [31,32]. The ceremonial center (Figure 3) became a place of periodic pilgrimage from places very far afield, preserving this function until about 450 CE [33].

Figure 3. Cahuachi ceremonial center. The mounds of Piramide Sur (background, on the left) and of the Gran Piramide (centre) are shown.

During this period, intense rains and associated mud-debris flows damaged the structures built with adobe bricks, sometimes involving the reconstruction of buildings among which was the Gran Piramide. Moreover, several authors have stated a strong link between the course of the Nasca civilization and the environmental conditions. As an example, Schittek et al. [34] stressed that the thriving period of the Nasca culture coincided with a relatively humid period while its demise coincided with an abrupt environmental turnover occurring at 1.3 ka. Up to about 0.8 ka, the lack of river activity is interpreted as due to renewed hyper-arid conditions, coinciding with the warm Medieval Climate Anomaly [35]. A further shift to relatively humid conditions is again indicated by the river activity and occurrence of landslides. This moist and hydrologically unstable period would last until the Little Ice Age [30].

3. Material and Method

Cahuachi consists of a number of naturally smoothed mounds forming the core of pyramids and temples made of adobe [36]. According to Grodzicki [7,8,37] the bedrock of Cahuachi is represented by Holocene alluvium, covering the Tertiary substratum, and includes three ENSO-related conglomerates, dated to the first century BCE, around 600 CE, and around 1000 CE, respectively. Each conglomerate would have been deposited by "slimy-crumbly flows" triggered by huge precipitation events. The upper and younger conglomerate was identified by Grodzicki on the Gran Piramide (Figure 4) and correlated with a similar strata visible in the northern area of the site. This latter was dated using organic material placed at its top [7,37]. In this way, this conglomeratic bed should cover all of the structures of Cahuachi up to 408 m a.s.l. [38].

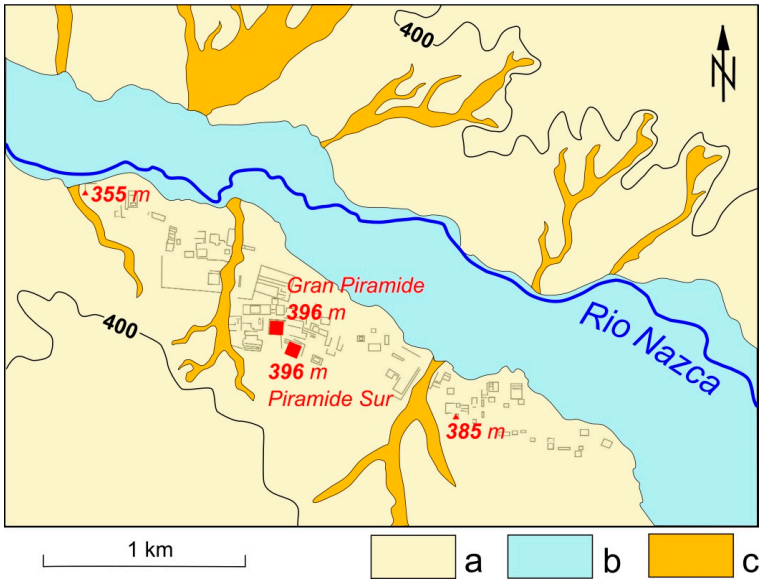

Figure 4. Geological map of Cahuachi. Legend: (a) Mudstones, sandstones and conglomerates; (b) alluvial deposits; (c) colluvium, debris flows; from [39], modified. 400 m a.s.l. contour line is reported. Gran Piramide and Piramide Sur are evidenced with red squares.

As mentioned above, an excavation close to the Piramide Sur (about 70 m south-east of the Gran Piramide, see Figure 4) carried out by the archaeological team of G. Orefici, has temporarily allowed the observation of a stratigraphic column of about 13 m (Figure 5). A close cavity (probably a type of food storage) has enabled us to extend the stratigraphic observations in depth for a total of 17 m [39].

The measured section is capped by a conglomerate corresponding to that described by Grodzicki [8,39] on the Gran Piramide and thus allows us to test his thesis. The stratigraphic observation was performed together with the collection of twelve samples for laboratory analysis.

The grain-size composition of the sediment samples was determined through dry sieving after overnight drying in an oven at 80 °C. Dried sediments were homogenized and classified according to the Wentworth scale grade [40] by passing through a stack of sieves with mesh apertures of 4 mm (granules), 2 mm (very coarse sand), 1 mm (coarse sand), 0.50 mm (medium sand), 0.25 mm (fine sand), and 0.063 mm (silt). These grain-size steps were then transformed into the logarithmic φ scale of Krumbein [41]. Weights (±0.0001 g) of the sediment fractions were used to determine the general grain-size distribution of the sediments. Moreover, the grain size data for all samples were reclassified into gravel, sand, and mud, and presented in a ternary diagram [42].

Mineralogic and petrographic investigations were carried out at the University of Urbino Carlo Bo using a polarized light optical microscope and a scanning electron microscope (SEM) FEI Quanta 200 FEG environmental scanning electron microscope (ESEM) equipped with an energy-dispersive X-ray spectrometer (EDAX) for semi-quantitative chemical analyses.

Figure 5. Panning shot of the excavation used to measure the stratigraphic section.

4. Results (Stratigraphic, Mineralogical and Petrographic Analysis)

4.1. Stratigraphy

The succession measured beneath the Piramide Sur had a sub-horizontal attitude and showed four subvertical joint systems, which were arranged according to angles of about 45°. Three main lithologies were recognized: greyish conglomerates and breccias, light brown sandstones, and light beige mudstones (Figure 6). In addition, a lithoid silty layer, a few centimeters thick, was found and sampled (CH3) at 6.5 m from the base.

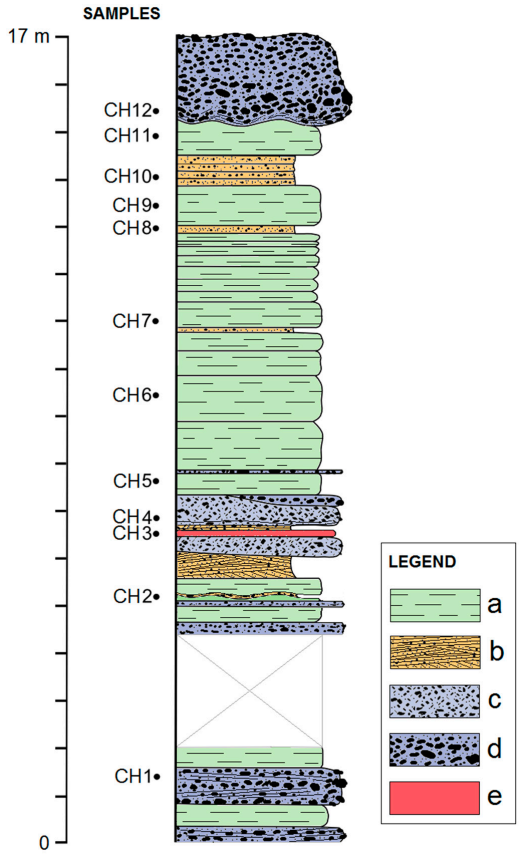

Figure 6. Piramide Sur stratigraphic section (from [39], modified). Legend: a, mudstone; b, sandstone; c, conglomerate with sharp clasts (breccia); d, conglomerate; e, lithoid siltstone.

The section ended just below the foundation of the temple, as indicated by the presence of mortar for adobe (Figure 7b). The stratification was plane-parallel except for some lenticular bodies and a few undulated lithological boundaries. Conglomerates prevailed at the lower half portion of the column while mudstones were more abundant at the upper half. The former presented imbrications of the pebbles, erosive basal contacts, and a sandy-muddy matrix. The pebbles generally showed degrees of sphericity from low to middle (Figure 7a). The thickest conglomerate measured 1.8 m, showed an abrupt undulated lower surface, and was placed at the top of the section (Figure 7b). Mudstones were either laminar or massive, but always poorly consolidated (Figure 7c). Load casts were observed at the upper surface of each stratum of mudstone overlaid by a conglomerate. Sandstones presented cross lamination (Figure 7d).

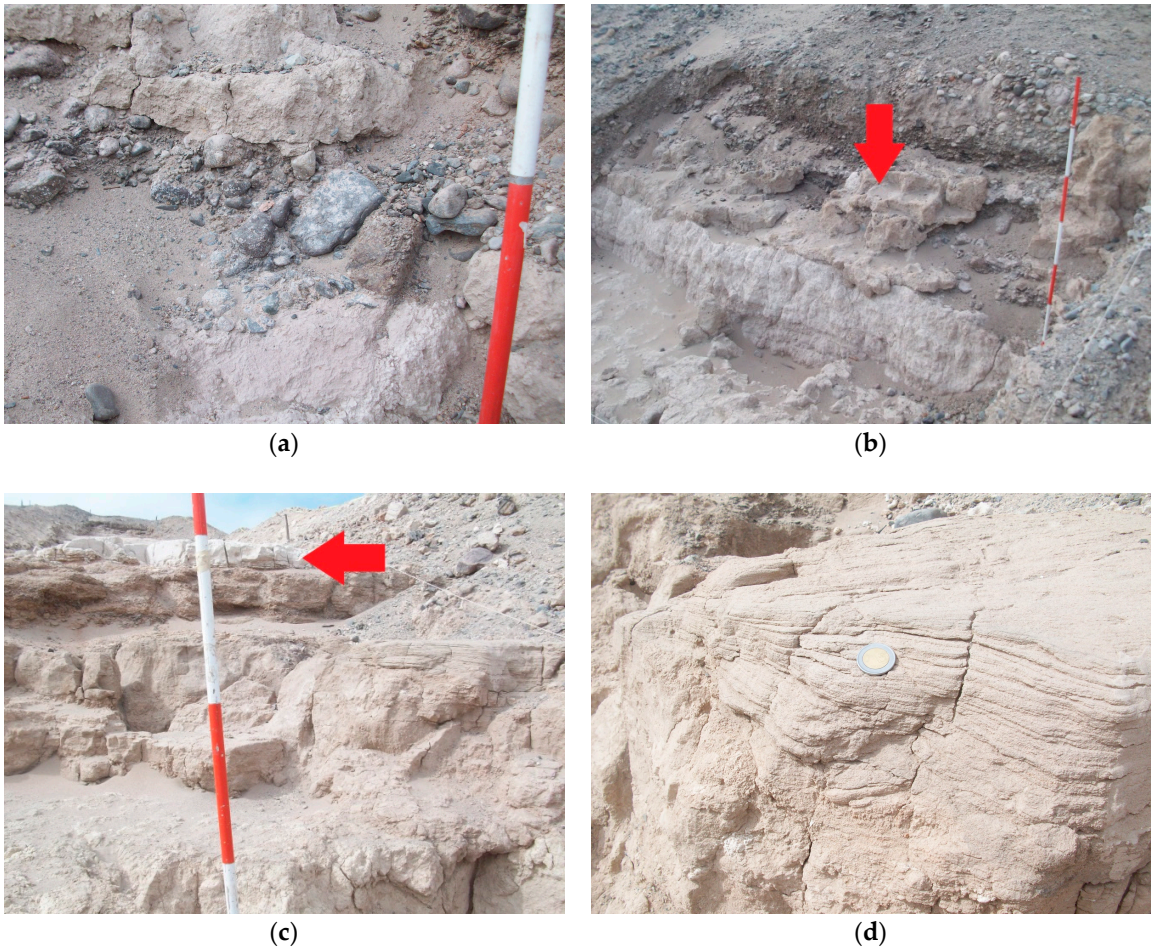

Figure 7. Stratigraphic features of the Piramide Sur section: (**a**) pebbles concentrations at the base of the upper conglomerate; (**b**) top of the section (1.8 m conglomerate overlays mudstone; mortar for adobes partially covers the contact); (**c**) the portion of the section comprised between 5 and 6.5 m from the section's base (it consists of mudstones and sandstones; note the whitish thin bed in the upper side); (**d**) a detail of cross-lamination in sandstone.

Sandy and silty fractions of the samples were screened on macro- and micro-fossil contents, but all tests gave a negative result.

4.2. Textural (Grain-Size) Characteristics

According to the stratigraphic description reported in the previous section, and applying the textural classification by Folk (1954), our analysis of the sediment grain-size (on the basis of the method of Wentworth, 1922, revisited on the logarithmic φ scale by Krumbein, 1934) shows that the lithologies

of Cahuachi are categorized into three groups: "sandy conglomerate", "muddy sandstone", and "sandy mudstone", with one sample (CH2) falling in the slightly conglomeratic muddy sandstone field (Table 1 and Figure 8). The majority of the sediment samples (46 vol.%) belong to the sandy mudstone group, while sandy conglomerate and muddy sandstones are present in a minor and comparable amount (27 vol.%). It is worth noting that one of the collected samples (CH3) was not processed for the grain size analysis because of its lithoid state; for this reason, it will be described as a separate sample (see next section). In addition, the statistic grain-size parameters of the sandy mudstones were not processed as the most abundant grain size fraction >4 φ (i.e., <63 microns) of this textural group was not separated into different grain-size classes for a correct cumulative curve.

Table 1. Grainsize distribution of the statistical parameters of studied sediments. SC = Sandy Conglomerate; SCMS = Slightly Conglomeratic Muddy Sandstone; SM = Sandy Mudstone; MS = Muddy Sandstone; PK_G = Platykurtic; MK_G = Mesokurtic; LK_G = Leptokurtic; VLK_G = Very Leptokurtic; PSo = Poorly Sorted; VPSo = Very Poorly Sorted; MSo = Moderately Sorted. n.d. = not determined.

Sample	Mean (Mz)	Median (Md)	Sorting (σ)	Skewness (Sk)	Kurtosis (K_G)	Remarks		Gravel (%)	Sand (%)	Mud (%)	Texture Group
CH1	0.51	0.55	1.77	0.04	0.74	PK_G	PSo	28.32	68.82	2.864	SC
CH2	1.67	1.73	2.2	0.08	1.25	LK_G	VPSo	8.008	78.77	13.23	SCMS
CH4	0.02	-0.38	1.93	0.46	1.33	LK_G	PSo	33.45	59.58	6.96	SC
CH5	n.d.	n.d.	n.d.	n.d.	n.d.	n.d.	n.d.	-	12.65	87.35	SM
CH6	n.d.	n.d.	n.d.	n.d.	n.d.	n.d.	n.d.	-	43.57	56.43	SM
CH7	n.d.	n.d.	n.d.	n.d.	n.d.	n.d.	n.d.	-	23.78	76.22	SM
CH8	2.88	2.69	1.25	0.4	1.76	VLK_G	MSo	-	86.06	13.94	MS
CH9	n.d.	n.d.	n.d.	n.d.	n.d.	n.d.	n.d.	-	26.41	73.59	SM
CH10	2.71	2.63	1.33	0.26	1.61	VLK_G	MSo	-	87.82	12.18	MS
CH11	n.d.	n.d.	n.d.	n.d.	n.d.	n.d.	n.d.	-	21.5	78.5	SM
CH12	−0.4	−1.10	1.69	0.67	1.04	MK_G	PSo	55.43	40.17	4.4	SC

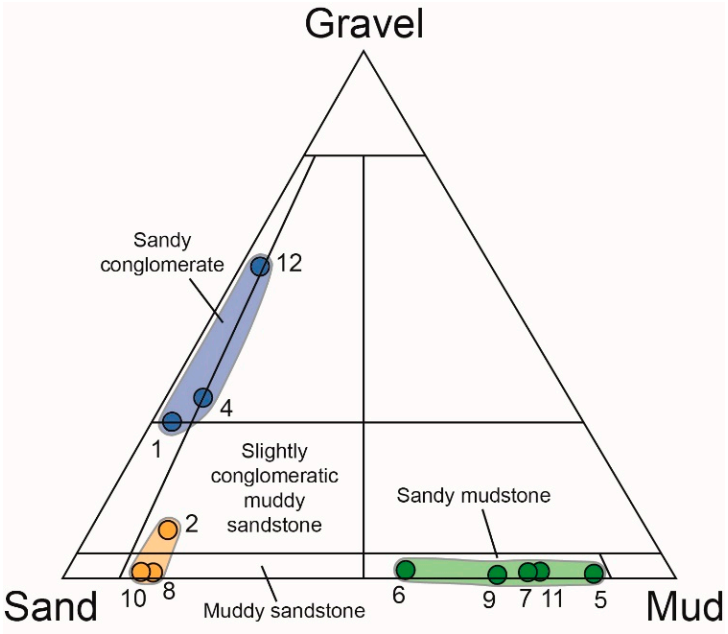

Figure 8. Ternary grain-size classification diagram proposed by Folk (1954), showing the proportion of mud, sand and gravel for the studied sediments collected at the Cahuachi site.

The grain size distribution patterns for the studied samples are graphically illustrated in Figures 9 and 10. According to the histograms in Figure 9, the sandy conglomerates show slightly bimodal distributions, with the main mode coinciding with the coarse modal class (−1 φ) and the second, minor mode moving to the finer classes (2 φ in the CH1 sample, >4 φ in the other samples). Muddy

sandstones are typically unimodal (3 φ), except for the CH2 sample, which showed a second, minor mode toward the finer classes (>4 φ). Sandy mudstones are typically fine-grained, always showing a significant mode for classes >4 φ. Mz values range from –0.4 to 0.51 φ in the sandy conglomerates and 1.67 to 2.88 φ in the muddy sandstones.

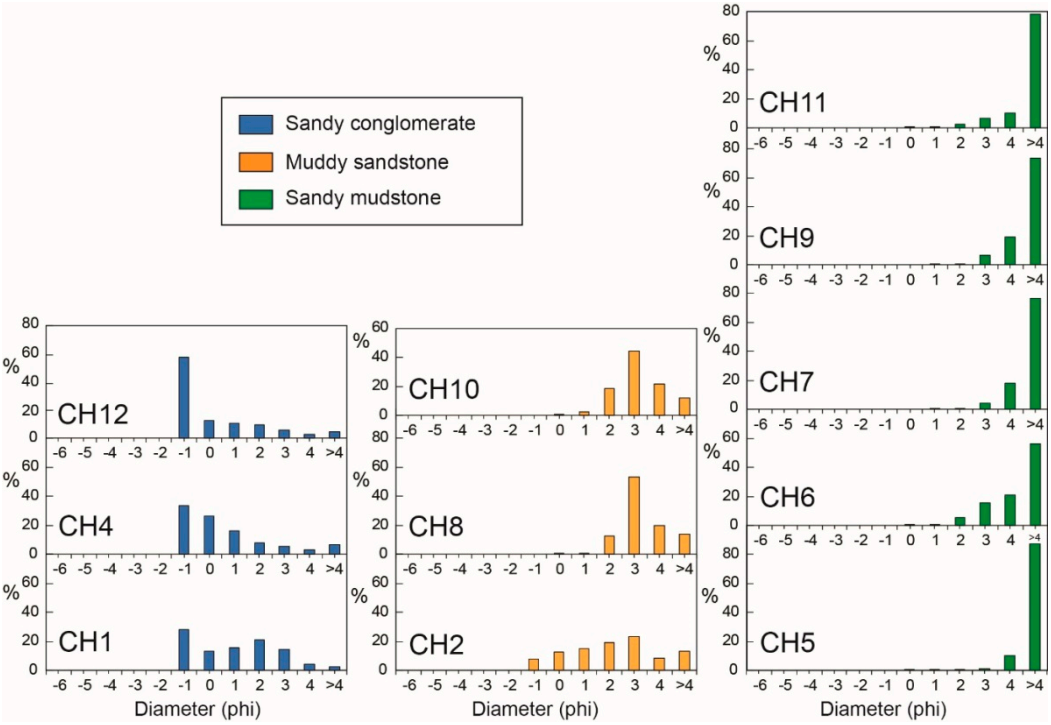

Figure 9. Histograms of the studied samples of Cahuachi.

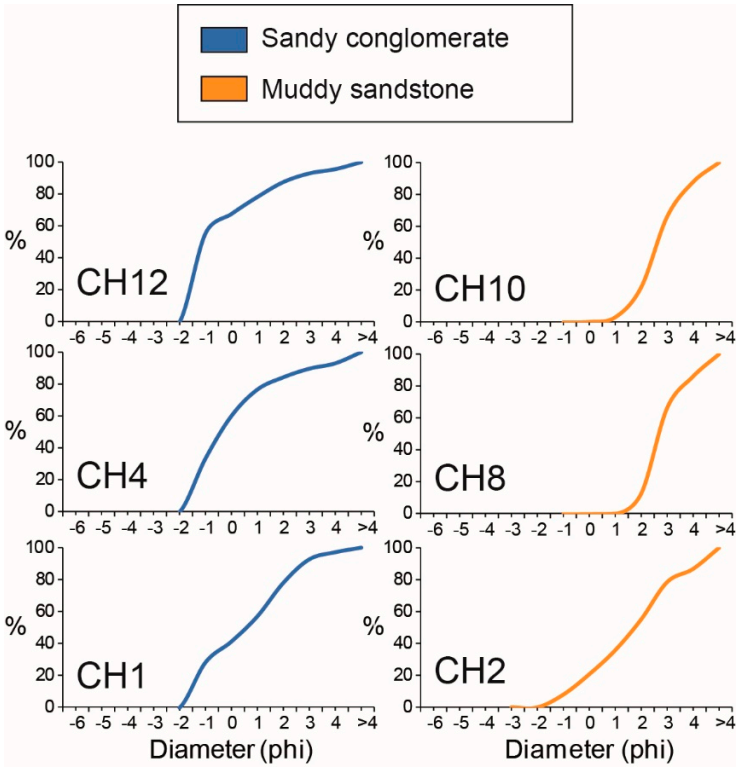

Figure 10. Cumulative curves showing the trends of the coarse-grained samples of Cahuachi.

On the basis of the cumulative curves, the median diameter (Md, i.e., 50th percentile) of the sandy conglomerates varies from 0.55 to –1.10 φ whereas that of the muddy sandstones ranges from 1.73 to 2.69 φ. The sorting value, mostly linked to the supply sources, to the energy of the environment, and the transport processes, varies from poorly sorted (1.69–1.93 φ) sandy conglomerates to moderately sorted (1.25–1.33 φ) muddy sandstones with the slightly conglomeratic muddy sandstone being very poorly sorted (2.2 φ).

The skewness values (Sk, indicating the deviation between Md and Mz) in the Cahuachi lithologies range from 0.04 to 0.67 φ in the sandy conglomerates, and from 0.08 to 0.4 φ in the muddy sandstones (this also includes the slightly conglomeratic muddy sandstone sample). Accordingly, all of these samples vary from near symmetrical to strongly positively skewed.

Regardings the Kurtosis parameter (K_G, showing the measure of the shape of the histogram curve, i.e., plate vs. tip), the studied samples also showed significant variability, with K_G ranging from platykurtic (0.74 φ, CH1), through to mesokurtic (1.04 φ, CH12) and leptokurtic (1.33 φ, CH4) in the sandy conglomerates. The muddy sandstones are very leptokurtic (1.61–1.76 φ), with the slightly conglomeratic muddy sandstone that is leptokurtic (1.25 φ).

4.3. Composition of the Volcaniclastic Layer CH3

Along the stratigraphic succession of Cahuachi, the lithoid silty layer (CH3) has a volcaniclastic origin. It placed above the two sandy conglomerates (CH1 and CH2), at the bottom of the stratigraphic section (Figure 6). This layer is composed of a predominant juvenile volcanogenic glass, associated with minor sialic and mafic volcanic crystals, and a scarce lithic fraction (Figure 11). The juvenile material consists of predominantly white pumices, marked by fluidal, spongy, and minor blocky texture, and fresh glass shards showing typical morphological features of explosive silicic magmatic eruptions (i.e., cuspate, plate, Y-shaped). Frequently, the delicate spines of bubble-wall and pumice shards are undeformed, suggesting that the shards were sufficiently cold at the moment of the depositional process of this volcaniclastic level. Igneous minerals include plagioclase, clinopyroxene, biotite, and Fe–Ti oxides. These generally occur as loose subhedral crystals, but they can also be found as phenocrysts/microphenocrysts in pumices and lithic clasts. The lithic fraction is mainly represented by fine-grained, vitropyric rock fragments. Some lithics contain phenocrysts of plagioclase and pyroxene in a groundmass consisting of the same phases and brown glass.

Semi-quantitative chemical analyses were carried out on selected mineral phases and glass shards in a thin polished section with an SEM (Figure 11). The composition of the analyzed plagioclase crystals roughly ranged from andesine to labradorite. Pyroxene was present as euhedral to subhedral crystals of augitic compositions, while mica was Mg-rich biotite.

This volcaniclastic level could represent a widespread tephrostratigraphic regional marker in the framework of the regional sedimentary sequences.

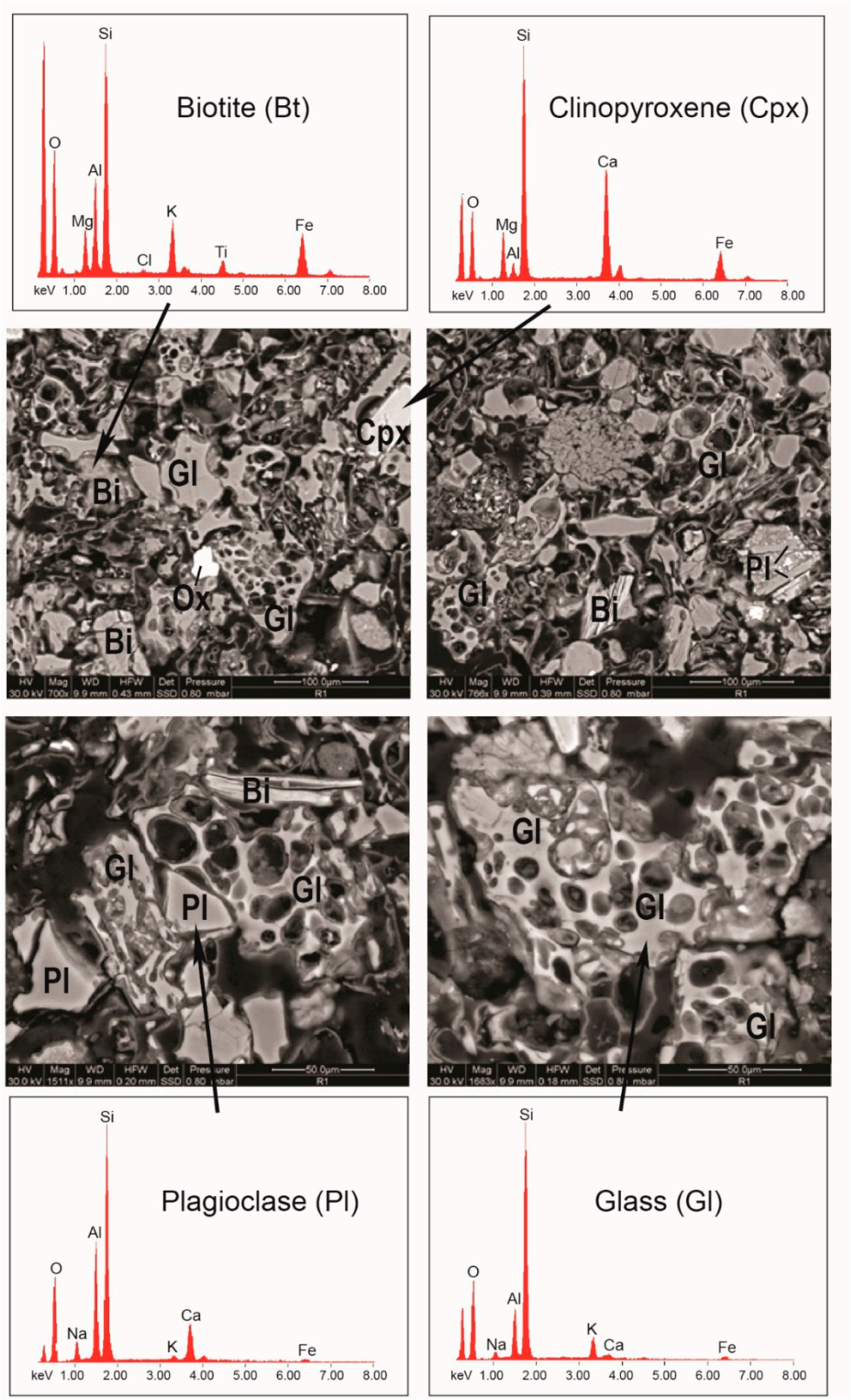

Figure 11. Scanning electron microscope (SEM) microphotographs and energy-dispersive X-ray spectrometer (EDAX) spectra of the studied volcaniclastic layer (CH3) from the Cahuachi succession. Gl = glass; Pl = plagioclase; Bi = biotite; Cpx = clinopyroxene; Ox = Fe-Ti oxides.

4.4. Petrography of Pebbles within the Sandy Conglomerates

Representative pebbles within the sandy conglomerate samples (CH1, CH4 and CH12) of the investigated Cahuachi succession were selected for thin section petrographic study by a polarized light optical microscope to determine their lithology. The sandy conglomerates contain pebbles of similar petrographic composition (Figure 12). The petrotypes observed can be referred to as sedimentary, magmatic, and metamorphic rocks. Sedimentary lithoclasts, mainly represented by siltites, arenites, quartz-arenites, and volcaniclastic arenites; magmatic lithoclasts (plutonic and volcanic) consisting of granites, granodiorites, diorites, andesites, dacites, and rhyolites (also comprising of vitrophyric pyroclasts); and metamorphic pebbles, composed of gneisses and schists. Fragments of vitrophyric pyroclasts are also abundant.

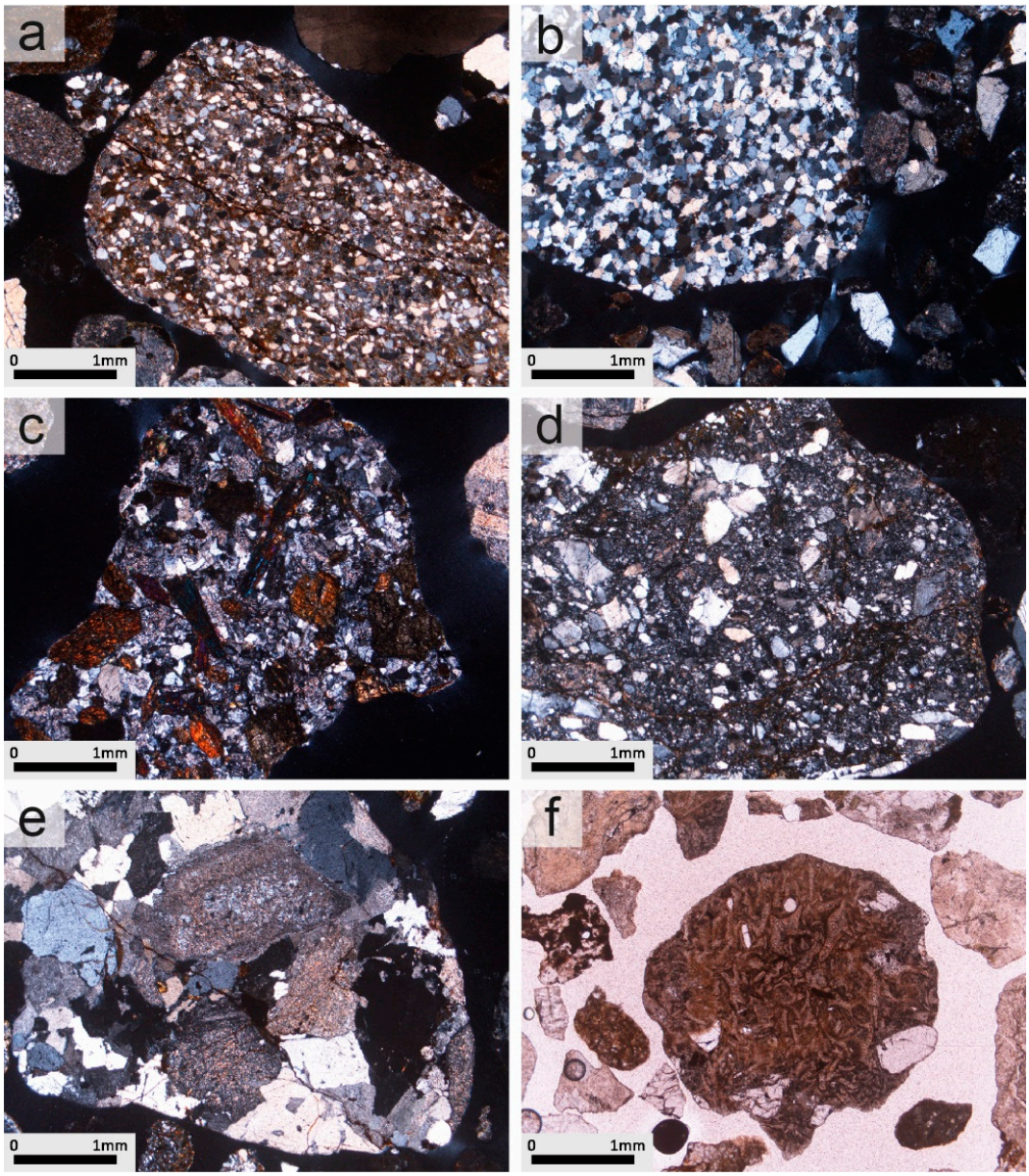

Figure 12. Thin section microphotographs (**a**–**e**: crossed nicols polarized light; **f**: simple polarized light) in of representative pebbles from the sandy conglomerates. **a** = arenite; **b** = quartz-arenite; **c** = intermediate (andesite-like) volcanic rock; **d** = acid (dacite-rhyolite-like) volcanic rock; **e** = granitoid (with feldspar crystals mostly altered to sericite and clay minerals); **f** = vitrophyric pyroclast.

The sedimentary lithoclasts are dominated by arenites and quartz-arenites, while siltites and volcaniclastic arenites are subordinate. Arenites and quartz-arenites (Figure 12a,b) show a mineralogically homogeneous texture dominated by very fine to coarse-grained quartz grains. The detrital grains are variable, but in general, are of a medium degree of roundness and sphericity. The quartz is predominantly monocrystalline and non-undulatory to weakly undulatory, but some grains exhibit undulose extinction or distinct zones of extinction with sharp boundaries (i.e., polygonized quartz). The amount of variously altered alkali feldspar is scarce and decreases passing from arenites to quartz-arenites. Granitoid rock fragments and carbonate lithics appeared in some thin-sections of the arenites. The siltite clasts show good sorting and appear with a massive and parallel laminated microstructure. The volcaniclastic sandstones, which are predominantly coarse-grained, contain a mixture of framework grain types including variably altered, coarse-grained porphyritic types with large euhedral feldspars, finely crystalline basaltic, and devitrified glassy grains, together with sub-rounded to angular detrital quartz grains.

The magmatic lithoclasts are mainly represented by granite, granodiorite, syenite, and volcanic rocks (andesites, dacites and rhyolites). These clasts occur as pebbles, with various roundness degrees. Pebbles of volcanic origin (Figure 12c,d) are typically sparsely to densely porphyritic, rarely aphyric with a glassy to a fine-grained matrix. Pale brownish clinopyroxene and amphibole are the dominant mafic phenocrysts. Plagioclase phenocrysts are abundant in the phenocrysts population, while either plagioclase or alkali feldspar could be part of the groundmass. The granites and the granodiorites are mostly characterized by the slight to strong alteration of feldspars into secondary minerals such as sericite and clay minerals (Figure 12e). Their microstructures are holocrystalline and hypidiomorphic granular. Diorite lithoclasts are subordinate (with respect to granitoids).

Metamorphic lithoclasts are very subordinate and are mainly represented by gneisses and schists. They show a variable schistose texture characterized by the parallel alignment of fine- to medium-grained mica flakes (mainly biotite, muscovite) intercalated with quartz, plagioclase, K-feldspar, and other minor minerals. Muscovite is generally more abundant than biotite in the schists, where it could be the only phyllosilicate.

Vitrophyric pebbles (Figure 12f) consist of colorless to brownish, vesicle-poor to pumiceous, silicic glass shards, euhedral crystals (feldspars and biotite), and altered volcanic lithic clasts. In some cases, these clasts are almost entirely formed by an assemblage of vitrophyric particles such as Y-shaped glass shards and glass fragments with sinuous or cuspate outlines, with subordinate subhedral to euhedral crystals.

5. Discussion, Summary and Outlook

The stratigraphic study of the Piramide Sur section (Figure 6) did not emphasize any fundamental discontinuity and therefore the section must belong to a single unit. This feature is not in agreement with the interpretation of Grodzicki [8,37] of the sandy conglomerate at the top as an ENSO-related deposit. Moreover, due to the lithological features, the whole succession of Figure 6 can be easily correlated to the regional succession, and in particular, to the upper part of the Changuillo Formation or the transitional stratigraphic level of the Changuillo–Canete Fms [23,43]. The surveyed features did not permit the correlation of the geological section to a well-defined depositional environment, however, one can hypothesize a depositional setting related to the progradation of alluvial fans.

The detection of mortar for adobe (for the constructive characteristics of the Piramide Sur Temple, see Orefici [44]) covering the top conglomerate at the Piramide Sur stratigraphic section (Figure 7b) requires some considerations. Near Gran Piramide, Grodzicki [8] asserted that the conglomerate covered a wall of adobe, thus supporting both its depositional interpretation and dating. Currently, clear contact between the conglomeratic layer and the adobe structure is not visible due to both the restoration works of the archaeological building and the thick level of eluvium constituted by gravel and sand coming from the conglomerate [39]. It is most likely that Grodzicki did not have good exposure of the bedrock and considered the conglomerate was a recent alluvial deposit under

the influence of a geomorphological aerial photo interpretation [45]. On the contrary, the top of the Piramide Sur section clearly shows the relation between the sandy conglomerate and the bottom of an adobe wall, thus constraining the pre-existence of the geological layer from which sample CH12 was collected.

An outlook to support the preliminary results of the present study should be to date the sandy conglomerates of the Cahuachi stratigraphic section using the optically stimulated luminescence (OSL) method to rule out the recent age supposed by Grodzicki [8,37]. The optical dating of sediments using OSL signals in mineral grains began in 1985 [46]. This exciting new technique dates deposition back to 200 ka or more and its applications cover many areas of Earth and environmental sciences, comprising archaeological and anthropologic contexts [47,48]. OSL has, in fact, the potential to determine the time elapsed since energy was trapped in the crystal structures as a result of exposure to natural ionizing radiation was last released by exposure to daylight (i.e., the time elapsed since the last transport and deposition of sediment). Minerals most commonly used in OSL are quartz and feldspar, which are virtually ubiquitous in terrestrial surface sedimentary settings. The technique complements other Quaternary dating methods of sedimentary succession including radiocarbon (^{14}C), uranium series methods, and cosmogenic nuclide techniques. Debris flow dating by OSL is currently used (e.g., [49] and references therein), although the opportunity for sufficient light exposure during debris flows is limited, and thus heterogeneous resetting of the latent OSL signal can be expected [50].

The texture and composition of the sandy conglomerates confirm the above lithostratigraphic correlation. On the basis of the petrographic composition of the pebbles, a very similar provenance area of the sandy conglomerates could be inferred for all three of the investigated samples (CH1, CH4 and CH12). Although CH12 is characterized by a relatively higher mean grain-size (Mz –0.4 with respect to 0.02–0.51 of CH1–CH4; Figure 8), all of the other textural parameters (Md, Sorting, Skewness, Kurtosis; Table 1; Figure 9) are comparable for the three sandy conglomerates. In particular, the similarity of the three cumulative curves (Figure 10) emphasize a poorly sorted character (σ 1.69–1.93 φ), indicating the similar energy of the sedimentary environment and transport processes. All of the above features, coupled with similar roundness for all of the pebbles, independent of their sedimentary, magmatic, or metamorphic origin, address the interpretation of the three sandy conglomerates as being derived from similar geological conditions of (i) supply area, (ii) transport, and (iii) kind of siliciclastic rocks, unlike their different position in the investigated stratigraphic sequence at Cahuachi (CH1—CH4, bottom; CH12, top). As a matter of fact, if the thesis of Grodzicki was right, significant textural and compositional differences should have occurred in the sandy conglomerate at the top, with respect to the other similar lithological levels throughout the investigated section. Moreover, the sandy conglomerates of Cahuachi are quite different to the El Niño catastrophic-flood signatures described in the literature [19–22,51].

The lithoid silty layer CH3 has a volcaniclastic origin as shown above. It is worth noting that some volcaniclastic layers have been reported at the upper portion of the Changuillo Fm [23,43], while no volcanic layer was detected in the recent surficial deposits at the *pampa* of Nazca [52]. However, this should be further verified by additional mineralogical and petrographic studies and detailed chronologic and tephrostratigraphic correlations on a regional scale among various sections of the Changuillo Fm. Tephra fingerprinting is widely recognized as a useful method for stratigraphic reconstructions across wide areas, which makes them a straightforward instrument for dating and correlating stratigraphic sections. This method is largely employed in the Quaternary (e.g., [53]) and has been used for correlating deposits of large eruptions of the Central Andes [54,55]. The abundant volcanic ashes interbedded with the basin-filling sedimentary succession provide a snapshot of the long-lived activity of Andean volcanoes of southern Peru, frequently punctuated by large explosive eruptions. In particular, fingerprints to correlate the tephra layer will be addressed with similar geochemical compositions, morphology of glass shards, and their grain-size, together with a detailed chronostratigraphic study using ^{39}Ar–^{40}Ar to date the biotite microlites that are ubiquitous in the erupted pyroclastic products of intermediate to high-silica compositions characterizing

subduction-related volcanism. Among the products of the continuous Neogene magmatic activity in southern Peru [56], our tephrostratigraphic investigations will focus on the ash layers derived from the Upper Barroso arc (between 3 and 1 Ma) as defined in the literature [57].

Our preliminary results on the stratigraphic, textural and petrographic study of the geological interval investigated at Cahuachi provide fundamental clues on the matching of the studied section with common regional successions (i.e., Changuillo– or Changuillo–Canete Formations) of the *pampa* of Nazca rather than the ENSO-related deposits described by Grodzicki [7,8]. Further investigation of the fine matrix particles (mostly clay minerals, work in progress) in the lithological units of the section of Cahuachi here reported, together with the study of all the sections reported by Grodzicki, should give additional constraints. The impact of the Mega El Niño events on southern Peru, especially those that occurred around 1000 CE, should be reconsidered in terms of our thesis, which will be reconciled with detailed chronological (e.g., tephrochronology) and biostratigraphic data [58,59].

Author Contributions: M.D.R. conceived the research and conducted the geological survey, the stratigraphic reconstruction and the sample collection work; M.M. and A.R. performed textural, mineralogical and petrographic analysis; N.C. analysed the stratigraphic data; M.D.R., M.M. and A.R. analysed the results, wrote and revised the manuscript.

Funding: This research was funded by the Department of "Scienze Pure e Applicate" (Università di Urbino) through the project "Enhancement of research 2017-2018" entitled "Il contributo delle Scienze della Terra nella definizione della scomparsa della civiltà *Nasca*: il caso di studio geoarcheologico dell'abbandono del sito cerimoniale di Cahuachi (Perù)", responsible A.R. The field survey was performed during the project "Italian Mission of Heritage Conservation and Archaeo-Geophysics (ITACA)", responsible N. Masini (Consiglio Nazionale delle Ricerche).

Acknowledgments: The authors would like to thank M. Bellagamba, S. Galeotti and F. Frontalini (Università di Urbino) for macro- and microfossils-check of the studied samples.

Conflicts of Interest: The authors declare no conflict of interest.

References

1. Magilligan, F.J.; Goldstein, P.S. El Niño floods and culture change: A late Holocene flood history for the Rio Moquegua, southern Peru. *Geology* **2001**, *29*, 431–434. [CrossRef]
2. Sandweiss, D.H. Terminal Pleistocene through mid-Holocene archaeological sites as paleoclimatic archives for the Peruvian coast. *Palaeogeogr. Palaeoclimatol. Palaeoecol.* **2003**, *194*, 23–40. [CrossRef]
3. Brooks, W.E.; Willett, J.C.; Kent, J.D.; Vasquez, V.; Rosales, T. The Muralla Pircada: An ancient Andean debris flow retention dam, Santa Rita B archaeological site, Chao Valley, northern Peru. *Landslides* **2005**, *2*, 117–123. [CrossRef]
4. Craig, A.K.; Shimada, I. El Niño flood deposits at Batan Grande, northern Peru. *Geoarchaeology* **1986**, *1*, 29–38. [CrossRef]
5. Uceda, C.S.; Canziani Amico, J. Evidencias de grandes precipitaciones en diversas etapas constructivas de la Huaca de la Luna, costa norte del Perú. *Bull. Inst. Fr. Études Andines* **1993**, *22*, 313–343. (In Spanish)
6. Contreras, D.A. Landscape and Environment: Insights from the Prehispanic Central Andes. *J. Archaeol. Res.* **2010**, *18*, 241–288. [CrossRef]
7. Grodzicki, J. Las catástrofes ecológicas en la Pampa de Nazca a fines del Holoceno y el fenómeno "El Niño". In Proceedings of the El fenómeno El Niño: A través de las fuentes arqueológicas y geológicas, Warsaw, Poland, 18–19 May 1990; Grodzicki, J., Ed.; Warsaw University; pp. 64–102. (In Spanish)
8. Grodzicki, J. Los geoglifos de Nasca segun algunos datos geologicos. In Proceedings of the Paleo ENSO Records, ORTOM-CONCYTEC Intern. Symp., Lima, Peru, March 1992; pp. 119–130. (In Spanish)
9. Macharé, J.; Ortlieb, L. Registros del fenomeno El Niño en el Perù. *Bull. Inst. Fr. Études Andines* **1993**, *22*, 35–52. (In Spanish)
10. Van Buren, M. The archaeology of El Niño events and others "natural" disasters. *J. Archaeol. Method Theory* **2001**, *8*, 129–149. [CrossRef]
11. Silverman, H. *Ancient Nasca Settlement and Society*; University of Iowa Press: Iowa City, IA, USA, 2002.

12. Moseley, M.; Tapia, J.; Satterlee, D.S.; Richardson, J.B. Flood events, El Niño events, and tectonic events. In Proceedings of the Paleo-ENSO Records Intern. Symp., Lima, Peru, March 1992; Ortlieb, L., Macharé, J., Eds.; Orstom-Concytec: Lima, Peru; pp. 207–212. (In Spanish)
13. Mörner, N.A. Present El Niño-ENSO events and past super-ENSO events. *Bull. Inst. Fr. Études Andines* **1993**, *22*, 3–12.
14. Keefer, D.K.; Moseley, M.E.; de France, S.D. A 38 000-year record of floods and debris flows in the Ilo region of southern Peru and its relation to El Niño events and great earthquakes. *Palaeogeogr. Palaeoclimatol. Palaeoecol.* **2003**, *194*, 41–77. [CrossRef]
15. Laoshuti, T.; Selover, D.D. Does El Niño affect business cycles? *East. Econ. J.* **2007**, *33*, 21–42. [CrossRef]
16. Cai, W.; Borlace, S.; Lengaigne, M.; Van Rensch, P.; Collins, M.; Vecchi, G.; Timmermann, A.; Santoso, A.; McPhaden, M.J.; Wu, L. Increasing frequency of extreme El Niño events due to greenhouse warming. *Nat. Clim. Chang.* **2014**, *4*, 111–116. [CrossRef]
17. Gutierrez, L. Impacts of El Niño-Southern Oscillation on the wheat market: A global dynamic analysis. *PLoS ONE* **2017**, *12*, e0179086. [CrossRef] [PubMed]
18. INGEMMET. *Mapa Geologico del Cuadrangulo de Palpa*; Ministerio de Energia y Minas: Lima, Peru, 1994.
19. Nials, F.L.; Deeds, E.E.; Moseley, M.E.; Pozorski, S.E.; Pozorski, T.G.; Feldman, R. El Niño: The catastrophic flooding of coastal Peru. *Field Mus. Nat. Inst. Bull.* **1979**, *50*, 4–14.
20. Nials, F.L.; Deeds, E.E.; Moseley, M.E.; Pozorski, S.E.; Pozorski, T.G.; Feldman, R. El Niño: The catastrophic flooding of coastal Peru. Part II. *Field Mus. Nat. Inst. Bull.* **1979**, *50*, 4–10.
21. Wells, L.E.; Noller, J.S. Holocene coevolution of the physical landscape and human settlement in northern coastal Peru. *Geoarchaeology* **1999**, *14*, 755–789. [CrossRef]
22. Beresford-Jones, D.G.; Arce Torres, S.; Whaley, O.Q.; Chepstow-Lusty, A.J. The role of *Prosopis* in ecological and landscape change in the Samaca Basin, lower Ica Valley, south coast Peru from the Early Horizon to the Late Intermediate Period. *Latin Am. Antiqu.* **2009**, *20*, 303–332. [CrossRef]
23. Leó, W.; Aleman, A.; Torres, V.; Rosell, W.; De La Cruz, O. *Estratigrafía, sedimentología y Evolución de la Cuenca Pisco Oriental*; Boletín serie D, n. 27; INGEMMET: Lima, Peru, 2008. (In Spanish)
24. Hall, S.R.; Farber, D.L.; Audin, L.; Finkel, R.C.; Mériaux, A.S. Geochronology of pediment surfaces in southern Peru: Implications for Quaternary deformation of the Andean Forearc. *Tectonophysics* **2008**, *459*, 186–205. [CrossRef]
25. Macharé, J. La marge continentale du Pérou: Régimes tectoniques et sédimentaires cénozoiques de l'avant-arc des Andes centrales. Thèse Doct. Sc., Université Paris XI, Orsay, France, 1987. (In French)
26. Sebrier, M.; Macharé, J. Observaciones acerca del Cuaternario de la Costa del Perù. Central. *Bull. Inst. Fr. Études Andines* **1980**, *9*, 5–22. (In Spanish)
27. Pulgar Vidal, J. Geografía del Perú. Las Ocho Regiones Naturales. Editorial Inca SA: Lima, Peru, 1987. (In Spanish)
28. Caviedes, C.N.; Fik, T.J. The Peru–Chile eastern Pacific fisheries and climatic oscillation. In *Climate Variability, Climate Change and Fisheries*; Glantz, M.H., Ed.; Cambridge University Press: Cambridge, UK, 1992; pp. 355–376.
29. Mächtle, B.; Unkel, I.; Eitel, B.; Kromer, B.; Schiegl, S. Molluscs as evidence for a Late Pleistocene and Early Holocene humid period in the northern Atacama desert, southern Peru (14.5° S). *Quat. Res.* **2010**, *73*, 39–47. [CrossRef]
30. Mächtle, B.; Eitel, B. Fragile landscapes, fragile civilizations—How climate determined societies in the pre-Columbian south Peruvian Andes. *Catena* **2013**, *103*, 62–73.
31. Orefici, G. *Nasca—Archeologia per una ricostruzione storica*; Jaka Book: Milan, Italy, 1992. (In Italian)
32. Orefici, G. Nasca historical and cultural analysis. In *Ancient Nasca World. New Insights from Science and Archaeology*; Lasaponara, R., Masini, N., Orefici, G., Eds.; Springer: Basel, Switzerland, 2016; pp. 65–86.
33. Orefici, G. The decline of Cahuachi and the end of the Nasca theocracy. In *Ancient Nasca World. New Insights from Science and Archaeology*; Lasaponara, R., Masini, N., Orefici, G., Eds.; Springer: Basel, Switzerland, 2016; pp. 449–468.
34. Schittek, K.; Forbriger, M.; Mächtle, B.; Schäbitz, F.; Wennrich, V.; Reindel, M.; Eitel, B. Holocene environmental changes in the highlands of the southern Peruvian Andes (14° S) and their impact on pre-Columbian cultures. *Clim. Past* **2015**, *11*, 27–44. [CrossRef]

35. Graham, N.E.; Hughes, M.K.; Ammann, C.M.; Cobb, K.M.; Hoerling, M.P.; Kennett, D.J.; Kennett, J.P.; Rein, B.; Stott, L.; Wigand, P.E.; et al. Tropical Pacific—Mid-latitude teleconnections in medieval times. *Clim. Chang.* **2007**, *83*, 241–285. [CrossRef]
36. Orefici, G. *Cahuachi. Capital Teocrática Nasca*; Fundo Editorial Universidad SMP: Lima, Peru, 2012. (In Spanish)
37. Grodzicki, J. *Nasca: Los Síntomas Geológicos del Fenómeno El Niño y sus Aspectos Arquelógicos*; Cesla series Estudios y Memorias, 12; Warsaw University: Warsaw, Poland, 1994. (In Spanish)
38. Valladares, R.; Denysse, P. El Sector CAH 04, Y8—EXP 108: Las funciones de la Plaza al Este de la Gran Pirámide en los complejos ceremoniales de Cahuachi (Nazca), Período Intermedio Temprano. Graduation Thesis, Pontificia Universidad Católica del Perú, Lima, Peru, 2007. (In Spanish)
39. Delle Rose, M. The geology of Cahuachi. In *Ancient Nasca World. New Insights from Science and Archaeology*; Lasaponara, R., Masini, N., Orefici, G., Eds.; Springer: Basel, Switzerland, 2016; pp. 47–64.
40. Wentworth, C.K. A scale of grade and class terms for clastic sediments. *J. Geol.* **1922**, *30*, 377–392. [CrossRef]
41. Krumbein, W.C. Size frequency distributions of sediments. *J. Sediment. Petrol.* **1934**, *4*, 65–77. [CrossRef]
42. Folk, R.L. The distinction between grain size and mineral composition in sedimentary rock nomenclature. *J. Geol.* **1954**, *62*, 344–356. [CrossRef]
43. Montoya, M.; Carcía, W.; Caldas, J. *Geología de los Cuadrángulos de Lomitas, Palpa, Nasca y Puquio*; Boletín Serie A 53; INGEMMET: Lima, Peru, 1994. (In Spanish)
44. Orefici, G. Recent discoveries in Cahuachi: The Templo Sur. In *Ancient Nasca World. New Insights from Science and Archaeology*; Lasaponara, R., Masini, N., Orefici, G., Eds.; Springer: Basel, Switzerland, 2016; pp. 363–374.
45. Ostaficzuk, S. Development stages of the Nazca morphological features as readible on aerial photos. In Proceedings of the El fenómeno El Niño: A través de las fuentes arqueológicas y geológicas, Warsaw, Poland, 18–19 May 1990; Grodzicki, J., Ed.; Warsaw University; pp. 49–65.
46. Huntley, D.J.; Godfrey-Smith, D.I.; Thewalt, M.L.W. Optical dating of sediments. *Nature* **1985**, *313*, 105–107. [CrossRef]
47. Aitken, M.J. *An Introduction to Optical Dating*; Oxford University Press: Oxford, UK, 1998.
48. Rhodes, E.J. Optically Stimulated Luminescence Dating of Sediments over the Past 200,000 Years. *Annu. Rev. Earth Planet. Sci.* **2011**, *39*, 461–488. [CrossRef]
49. Zhao, Q.; Thomsen, K.J.; Murray, A.S.; Wei, M.; Song, B. Single-grain quartz OSL dating of debris flow deposits from Men Tou Gou, south west Beijing, China. *Quat. Geochronol.* **2017**, *41*, 62–69. [CrossRef]
50. Olley, J.; Caitcheon, G.; Murray, A. The distribution of apparent dose as determined by Optically Stimulated Luminescence in small aliquots of fluvial quartz: Implications for dating young sediments. *Quat. Sci. Rev.* **1998**, *17*, 1033–1040. [CrossRef]
51. Well, L.E. Holocene history of the El Niño phenomenon as recorded in flood sediments of northern coastal Peru. *Geology* **1990**, *18*, 1134–1137. [CrossRef]
52. Zavala, B.; Velarde, T. *Caracterización Geológica de los Depositos Superficiales en las Pampas de Nazca, Lineas y Geoglifos de Nazca, Informe Técnico—Geologia Ambiental y Riesgo Geolócico*; INGEMMET: Lima, Peru, 2008. (In Spanish)
53. Lowe, D.J.; Pearce, N.J.; Jorgensen, M.A.; Kuehn, S.C.; Tryon, C.A.; Hayward, C.L. Correlating tephras and cryptotephras using glass compositional analyses and numerical and statistical methods: Review and evaluation. *Quat. Sci. Rev.* **2017**, *175*, 1–44. [CrossRef]
54. Lebti, P.P.; Thouret, J.C.; Wörner, G.; Fornari, M. Neogene and Quaternary ignimbrites in the area of Arequipa, Southern Peru: Stratigraphical and petrological correlations. *J. Volcanol. Geotherm. Res.* **2006**, *154*, 251–275. [CrossRef]
55. Breitkreuz, C.; de Silva, S.L.; Wilke, H.G.; Pfander, J.A.; Renno, A.D. Neogene to Quaternary ash deposits in the Coastal Cordillera in northern Chile: Distal ashes from supereruptions in the Central Andes. *J. Volcanol. Geotherm. Res.* **2013**, *269*, 68–82. [CrossRef]
56. Thouret, J.C.; Jicha, B.R.; Paquette, J.L.; Cubukcu, E.H. A 25 myr chronostratigraphy of ignimbrites in south Peru: Implications for the volcanic history of the Central Andes. *J. Geol. Soc. Lond.* **2016**, *173*, 734–756. [CrossRef]
57. Mamani, M.; Wörner, G.; Sempere, T. Geochemical variations in igneous rocks of the Central Andean orocline (13°S to 18°S): Tracing crustal thickening and magma generation through time and space. *Geol. Soc. Am. Bull.* **2010**, *122*, 162–182. [CrossRef]

58. Delle Rose, M.; Renzulli, A. Overcoming the paradigm of the destruction of Nasca culture due to a Mega-El Niño event: A clue from the stratigraphic survey at Cahuachi (Peru). *Rendiconti online della Società Geologica Italiana* **2014**, *31*, 96.
59. Delle Rose, M.; Orefici, G.; Capuano, N.; Galassi, G.; Mattioli, M.; Santini, S.; Spada, G.; Renzulli, A. The decline of the Nasca culture (Peru) as the result of an increasing environmental stress: Overcoming the paradigm formulated at Cahuachi of catastrophic mega-floods due to El Niño-Southern Oscillation. In Proceedings of the 2018 SGI-SIMP Congress, Catania, Italy, 12–14 September 2018.

© 2019 by the authors. Licensee MDPI, Basel, Switzerland. This article is an open access article distributed under the terms and conditions of the Creative Commons Attribution (CC BY) license (http://creativecommons.org/licenses/by/4.0/).